OFFICE OF NAVAL RESEARCH

Technical Report No. 20

Adsorption of Pyridine at the Au(311) - Solution Interface

by

L. Stolberg, J. Lipkowski, and D.E. Irish

Prepared for Publication

in

Journal of Electroanalytical Chemistry

Guelph-Waterloo Center for Graduate Work in Chemistry
Waterloo Campus
Department of Chemistry
University of Waterloo
Waterloo, Ontario
Canada, N2L 3G1

DTIC
ELECTE
MAR 15 1991
S B D

February 15, 1991

AD-A232 823

91 3 11 046

REPORT DOCUMENTATION PAGE

1a REPORT SECURITY CLASSIFICATION Unclassified		1b RESTRICTIVE MARKINGS			
2a. SECURITY CLASSIFICATION AUTHORITY Unclassified		3. DISTRIBUTION/AVAILABILITY OF REPORT Public Release/Unlimited			
2b DECLASSIFICATION/DOWNGRADING SCHEDULE					
4. PERFORMING ORGANIZATION REPORT NUMBER(S) ONR Technical Report #20		5. MONITORING ORGANIZATION REPORT NUMBER(S)			
6a. NAME OF PERFORMING ORGANIZATION D. E. Irish University of Waterloo	6b OFFICE SYMBOL (If applicable)	7a NAME OF MONITORING ORGANIZATION Office of Naval Research			
6c. ADDRESS (City, State, and ZIP Code) Department of Chemistry University of Waterloo Waterloo, Ontario, Canada, N2L 3G1		7b. ADDRESS (City, State, and ZIP Code) The Ohio State University, Research Center 1314 Kinnear Road, Room 318 Columbus, Ohio, U.S.A., 43212-1194			
8a. NAME OF FUNDING/SPONSORING ORGANIZATION Office of Naval Research	8b OFFICE SYMBOL (If applicable)	9 PROCUREMENT INSTRUMENT IDENTIFICATION NUMBER N00014-87-J-1118			

8c ADDRESS (City, State, and ZIP Code) Chemistry Division 800 N. Quincy Street Arlington, VA, U.S.A., 22217-5000	10 SOURCE OF FUNDING NUMBERS			
	PROGRAM ELEMENT NO	PROJECT NO.	TASK NO	WORK UNIT ACCESSION NO

11 TITLE (Include Security Classification)

Adsorption of Pyridine at the Au(311) - Solution Interface

12 PERSONAL AUTHOR(S)
L. Stolberg, J. Lipkowski, and D.E. Irish

13a TYPE OF REPORT Technical	13b TIME COVERED FROM 08/90 TO 12/90	14. DATE OF REPORT (Year, Month, Day) 1990-02-15	15. PAGE COUNT 38

16. SUPPLEMENTARY NOTATION

Submitted to Journal of Electroanalytical Chemistry

17	COSATI CODES		18 SUBJECT TERMS (Continue on reverse if necessary and identify by block number)
FIELD	GROUP	SUB-GROUP	Pyridine adsorption on Au(311); chronocoulometry; relative Gibbs surface excess; electrochemistry

19. ABSTRACT (Continue on reverse if necessary and identify by block number)

The energetics of pyridine adsorption onto a Au(311) single crystal electrode surface have been investigated using chronocoulometry. Adsorption parameters such as the relative Gibbs surface excesses, the Gibbs energies of adsorption, and electrosorption valencies have been determined. The data have been analyzed in terms of both the electrode potential and surface charge density. Over the potential region investigated (-0.8 V to +0.6 V), pyridine has been found to adsorb in the vertical orientation with the nitrogen end of the pyridine molecule facing the Au(311) surface. The limiting surface concentration for this orientation was found to be $6.6 \pm 0.3 \times 10^{-10}$ mol cm^{-2}. The Gibbs energies of adsorption were calculated using the Henry's Law isotherm. At the potential of maximum adsorption, ΔG^O_{max} was found to be equal to -44 kJ mol^{-1}. The absolute value for ΔG^O_{max} is fairly large indicating that pyridine is weakly chemisorbed onto the Au(311) electrode surface.

20 DISTRIBUTION/AVAILABILITY OF ABSTRACT ☑ UNCLASSIFIED/UNLIMITED ☐ SAME AS RPT ☐ DTIC USERS	21 ABSTRACT SECURITY CLASSIFICATION Unclassified	
22a NAME OF RESPONSIBLE INDIVIDUAL Dr. Robert J. Nowak	22b. TELEPHONE (Include Area Code) (519) 885-1211, ext. 2500	22c. OFFICE SYMBOL

DD FORM 1473, 84 MAR   83 APR edition may be used until exhausted.   SECURITY CLASSIFICATION OF THIS PAGE
All other editions are obsolete.

Unclassified

ADSORPTION OF PYRIDINE AT THE AU(311)-SOLUTION INTERFACE

L. Stolberg[1,2], J. Lipkowski[1] and D.E. Irish[2]

Guelph-Waterloo Centre for Graduate Work in Chemistry
[1]Department of Chemistry and Biochemistry
University of Guelph
Guelph, Ontario, Canada N1G 2W1

[2]Department of Chemistry
University of Waterloo
Waterloo, Ontario, Canada N2L 3G1

Abstract

The energetics of pyridine adsorption onto a Au(311) single crystal electrode surface have been investigated using chronocoulometry. Adsorption parameters such as the relative Gibbs surface excesses, the Gibbs energies of adsorption, and electrosorption valencies have been determined. The data have been analyzed in terms of both the electrode potential and surface charge density. Over the potential region investigated (-0.8 V to +0.6 V), pyridine has been found to adsorb in the vertical orientation with the nitrogen end of the pyridine molecule facing the Au(311) surface. The limiting surface concentration for this orientation was found to be $6.6 \pm 0.3 \times 10^{-10}$ mol cm^{-2}. The Gibbs energies of adsorption were calculated using the Henry's Law isotherm. At the potential of maximum adsorption, ΔG^{o}_{max} was found to be equal to -44 kJ mol^{-1}. The absolute value for ΔG^{o}_{max} is fairly large indicating that pyridine is weakly chemisorbed onto the Au(311) electrode surface.

Introduction

This is the fifth paper in a series which is devoted to the study of the influence of crystallographic orientation of gold electrodes on the adsorption of pyridine from aqueous electrolyte solutions. In previous communications the adsorption of pyridine onto polycrystalline gold (1,2), Au(100) (3), Au(110) (4), and Au(111) (5) have been described. In this contribution the adsorption of pyridine onto a Au(311) single crystal electrode surface is reported. Chronocoulometry has allowed quantitative characterization of pyridine adsorption onto Au(311). Thus, adsorption isotherms, Gibbs energies of adsorption, and electrosorption valencies will be presented. The orientation of the pyridine molecules on the Au(311) electrode surface has been determined and will be discussed. Also, the adsorption of pyridine on the (311) and (110) faces of gold will be compared.

Experimental

The experimental procedures used in this work have been described in preceding communications (1-4). The working electrode was a Au(311) single crystal rod (99.99%, Johnson Matthey) with a cross sectional area of $0.0659\ cm^2$. Prior to each experiment the working electrode was flamed and then quenched with Milli-Q water.

All solutions were prepared from Milli-Q water (Waters). The supporting electrolyte was 0.1 M $KClO_4$. The $KClO_4$ (ACS Certified, Fisher) was purified by first calcinating, then recrystallizing twice from Milli-Q water and drying. Pyridine (ACS

Certified, Fisher) was used without further purification. Pyridine solutions ranging in concentration from 5×10^{-6} M to 2×10^{-3} M were investigated. Solutions were prepared from a 0.1 M pyridine stock solution. All solutions were deaerated with argon and during the experiment argon was passed over the top of the solution. Potentials were measured with respect to the external saturated calomel reference electrode (SCE). The counter electrode was a gold coil. The experiments were carried out at 25 ± 1 $^{\circ}$C.

The instrumentation and the sequence of the different steps involved in the data acquisition and processing have been described in previous papers. The experimental strategy involved characterization of the surface by recording cyclic voltammetry and differential capacity curves and quantitative determination of the electrode charge density, σ_M, from chronocoulometric experiments (1,3,6,7). These charge density data allowed the determination of the relative Gibbs excesses, the Gibbs energies of adsorption, and the electrosorption valencies.

Cyclic Voltammetry

Figure 1 shows cyclic voltammograms which have been recorded for Au(311) in the absence (a) and presence (b) of pyridine. The cyclic voltammograms presented here span the potential region -0.8 V to +1.1 V and were recorded for a sweep rate of 20 mV s^{-1}. It was always observed that cyclic voltammograms which superimpose from one cycle to the next could be obtained after 3 to 5 cycles when recorded immediately after contact between the crystal and the electrolyte solution was made. No distortion of

3

the curves due to the creeping effect or the presence of oxygen could be detected. This suggests that the solutions being investigated were always of high purity and free of oxygen.

Figure 1a shows that the double layer region extends from -0.8 V to +0.6 V. Therefore, pyridine adsorption studies on Au(311) will be restricted to this potential region. For potentials more negative than -0.8 V hydrogen evolution on Au(311) begins while for potentials more positive than +0.6 V oxidation of the gold surface takes place. Two peaks at +0.8 V and +1.02 V characterize the oxide forming region. On the reverse, negative scan, one can see that the reduction process is characterized by two peaks at +0.31 V and +0.73 V. Overall, the cyclic voltammogram presented here for Au(311) in the presence of 0.1 M $KClO_4$ is in good agreement with the cyclic voltammogram reported by Hamelin (8) for Au(311) in the presence of 0.01 M NaF. However, the peak at +0.73 V was not observed by Hamelin. This peak is connected with a change of pH in the vicinity of the electrode. It appears if the electrolyte solution is not buffered and/or stirred. We did not stir our solution while Hamelin did. This explains the difference between the present results and those of Hamelin.

Shown in Fig. 1b is a cyclic voltammogram which was recorded for Au(311) in the presence of 3×10^{-4} M pyridine + 0.1 M $KClO_4$. In the double layer region pyridine adsorption/desorption peaks can be seen. These peaks first become visible once the pyridine concentration reaches 7×10^{-5} M. The oxide formation region, as Fig. 1b

4

shows, is now characterized by a single broad peak at +0.97V. A shallow shoulder can be seen on the negative side of this peak. Changes in the appearance of the oxide formation region can be seen for pyridine concentrations as low as 7×10^{-6} M.

Differential Capacity

Presented in Fig. 2 are several differential capacity curves which have been recorded for Au(311) in both the absence and presence of pyridine. In each case the sweep rate was 5 mV s^{-1} and only the scan which was recorded in the direction of positive potentials is shown. On the reverse, negative scan, hysteresis was observed over the entire potential region investigated irrespective of whether pyridine was absent or present in the solution. The differential capacity curve recorded for Au(311) in the presence of 0.1 M KClO$_4$ displays a diffuse layer minimum at +0.020 ± 0.010 V which corresponds to the potential of zero charge (pzc); this value is in very good agreement with the value of +0.01 ± 0.01 V reported recently by Lecoeur et al. (9).

Figure 2 also shows differential capacity curves which were recorded for Au(311) in the presence of pyridine. The differential capacity curve recorded for the 10^{-4} M pyridine solution displays a broad peak at negative electrode potentials. When the pyridine concentration is increased to 10^{-3} M (or 2×10^{-3} M) this peak becomes sharp and a shoulder appears on its negative side. Both the position and the height of the peak are sensitive to the bulk pyridine concentration suggesting that this peak is characteristic of the adsorption/desorption of pyridine. At positive electrode potentials,

and for the two highest pyridine concentrations presented in this figure, a broad shallow hump is visible. It will be shown later that within this potential region the surface concentration of pyridine has reached a maximum saturation value, Γ_{max}.

For the most negative potentials shown in Fig. 2, and for bulk pyridine concentrations $\leq 2 \times 10^{-3}$ M, the differential capacity curves merge with the capacity curve recorded for the pure supporting electrolyte solution. This behaviour indicates that, at the negative potential limit (-0.8 V), the pyridine molecules are desorbed from the Au(311) electrode surface. In the present work pyridine adsorption studies were restricted to pyridine concentrations in the range 5×10^{-6} M to 2×10^{-3} M. The lower limit is determined by the slow mass transport of the pyridine molecules to the electrode surface. The upper limit is determined by the requirement that the pyridine molecules are desorbed from the electrode surface before the onset of the hydrogen evolution reaction.

Charge-Potential Plots

In order to acquire quantitative data for the adsorption process potential step experiments were carried out. These involved the following steps: (1) the electrode was initially held at a potential (initial potential) at which pyridine adsorption takes place for a period of time long enough to establish a state of equilibrium between the interface and the bulk of the solution (approximately 1.5 min.); (2) the potential was stepped to the value E = -0.8 V (final potential) at which a total desorption takes place (see Fig. 2) and the current transient corresponding to the charging of the interface was recorded. The

6

charging current was digitally integrated and the absolute charge density, σ_M, at the initial potential was calculated using the procedure described in refs. 1,3, and 7.

Shown in Fig. 3 are the absolute charge density-potential curves which have been obtained for Au(311) in both the absence and presence of pyridine. Pyridine concentrations ranging from 5×10^{-6} M to 2×10^{-3} M are shown in this figure. The reproducibility of the charge data was always checked and found to be within 1%. In the region which corresponds to the most negative electrode potentials studied, the σ_M - E curves for the various pyridine solutions are observed to merge with the curve obtained for the supporting electrolyte. This indicates that, for E < -0.7 V, the pyridine molecules are completely desorbed from the Au(311) electrode surface. This result is consistent with the differential capacitance measurements presented earlier in Fig. 2. For more positive values of E the absolute charge densities become strongly dependent upon the bulk pyridine concentration. Within this region the surface concentration of pyridine is an increasing function of the electrode potential. Following this region, the absolute charge densities, which are now positive, are essentially concentration independent indicating that the surface concentration of pyridine reached a maximum (saturation) value Γ_{max}. This region is characterized by a quasi-plateau. Initially, in this section of the curve, σ_M depends almost linearly on the electrode potential. Extrapolation of this segment of the curve to $\sigma_M = 0$ allowed us to determine the shift of the potential of zero charge, E_N. The value for E_N was found to be -0.73 ± 0.025 V. It can be shown that this value for

7

E_N indicates that the pyridine molecules are orientated on the Au(311) electrode surface in the vertical position with the nitrogen atom facing the metal surface (3-5). The section of the σ_M versus E curve, for which σ_M is independent of the bulk pyridine concentration, intersects the curve which was obtained for the supporting electrolyte at a unique value of the electrode potential and charge density. These values, which correspond to the potential and charge of maximum adsorption are: $+0.39 \pm 0.01$ V and $+27.6 \pm 0.4$ μC cm^{-2}, respectively.

Film and Surface Pressure Curves

Following the procedure outlined in ref. 1, the charge density versus potential curves were integrated and the pressure of the film of adsorbed pyridine (π) calculated. Shown in Fig. 4 are the film pressure versus electrode potential curves which have been obtained for the various pyridine concentrations studied. All of the curves are bell shaped and display a well defined maximum.

Independently, the surface pressures, ϕ, were calculated as a function of the charge density at the metal surface using the Parsons function ξ (i.e., $\xi = \gamma + \sigma_M E$ and $\phi = \xi_{\theta = 0} - \xi_{\theta = 1}$) (10). In this way the thermodynamic analysis of the data was carried out also using charge as the independent electrical variable. Shown in Fig. 5 are plots of ϕ versus σ_M for the various pyridine concentrations indicated. The surface pressure curves, like the film pressure curves presented above in Fig. 4, are bell shaped. Thus, the results in Figs. 4 and 5 are qualitatively similar. As expected, and for a given pyridine

concentration, the maximum value observed on the surface pressure curve is very similar to the maximum value observed on the corresponding film pressure curve.

The film and surface pressures reach fairly large values (> 100 mN m^{-1}) for moderate to high pyridine concentrations. This indicates that the zero coverage Gibbs energy of adsorption and/or the energy of attractive lateral interactions are also large.

Adsorption Isotherms

By differentiating the film pressure versus natural logarithm of the bulk pyridine concentration curves, the relative Gibbs excesses were calculated (1). Shown in Fig. 6a are plots of the relative Gibbs excess as a function of the applied potential for the various pyridine concentrations studied. Shown in Fig. 6b are the adsorption isotherms (Γ versus ln(c)) which have been obtained at constant potential. Figures 7a and 7b show the corresponding curves determined using charge density as the independent electrical variable. The Γ versus E or σ_M plots have a sigmoidal shape with one inflection point indicating that the adsorbed pyridine molecules assume only one orientation at the Au(311) electrode surface. The curves display a long well defined plateau which corresponds to a limiting surface concentration equal to 6.6 ± 0.3 x 10^{-10} mol cm^{-2}. This value is in good agreement with the packing density expected for a surface covered by a monolayer of pyridine molecules orientated in the vertical position (11).

The adsorption isotherms determined at constant potential (Fig. 6b) are steep. In contrast, the isotherms plotted at constant σ_M (Fig. 7b) have very small slopes.

Consequently, the shape of the adsorption isotherm is essentially determined by the choice of the electrical variable. Any attempt to discuss these curves in terms of molecular models leading to an equation of an adsorption isotherm would give contradictory conclusions. Therefore, no isotherm has been used to describe the present results.

Gibbs Energy of Adsorption

In the potential range -0.5 V to 0 V the Gibbs energies of adsorption, ΔG^o, were calculated from the initial slopes of the π versus mole fraction of pyridine plots using the expression for Henry's Law as explained in ref. 3. A value of Γ_{max} equal to 6.6 x 10^{-10} mol cm^{-2} was used in the calculations. For potentials more positive than 0 V, the surface concentration of pyridine is equal to Γ_{max} even for the lowest bulk pyridine concentrations investigated. Under these conditions the Henry's Law coefficients could not be determined from the slopes of the π versus mole fraction of pyridine plots. To evaluate the Gibbs energies of adsorption at more positive potentials the π values were plotted against RTln(c) at constant E for potentials in the region 0 V to +0.5V. The plots were linear and parallel to each other. These plots were than shifted by a distance RTΔln(c) along the RTln(c) axis to give the best overlap with the curve for E = 0 V. The magnitude of RTΔln(c) was than taken as equal to the difference between the Gibbs energies at E = 0 V and at a given potential E.

Shown in Fig. 8 is a plot of ΔG^O versus E. The standard state is unit mole fraction of pyridine in the bulk of the solution and unit coverage at the surface (unsymmetrical choice of standard state (12)). The data presented in Fig. 8 span the potential region -0.7 V to +0.5 V. As Fig. 8 shows, the ΔG^O versus E relationship is parabolic in nature. The maximum value observed for ΔG^O is -44 kJ mol^{-1}. This fairly large value for ΔG^O_{max} indicates that the pyridine molecules are weakly chemisorbed onto the Au(311) electrode surface.

The electrosorption valency, γ', is equal to the first derivative of the ΔG^O versus E plot. Independently, the electrosorption valency can also be determined from the dependence of the charge density on the surface concentration taken at constant electrode potential by using the following relationship (13):

$$\gamma' = \frac{1}{F}\left(\frac{\partial \mu_p}{\partial E}\right)_\Gamma - \frac{1}{F}\left(\frac{\partial \Delta G^o}{\partial E}\right)_\Gamma = -\frac{1}{F}\left(\frac{\partial \sigma_M}{\partial \Gamma}\right)_E \tag{1}$$

Therefore, the slopes of the σ_M versus Γ plots can be compared to the first derivative of the ΔG^O versus E plot to check the consistency of our results.

Presented in Fig. 9 are plots of σ_M versus Γ which have been obtained at constant electrode potential. The data presented in this figure span the potential region -0.55 V to -0.05 V. As this figure shows, quasilinear relationships are observed although the spread of the experimental points is fairly large. The electrosorption valencies determined from the slopes of these plots are shown in Fig. 10. Independently, the ΔG^O

11

versus E data of Fig. 8 were fitted by a polynomial of the 2nd order and numerically differentiated. The electrosorption valencies determined by this method are also plotted in Fig. 10. The two sets of data agree with each other fairly well. This shows that our data display an internal consistency and that no major errors were made in the data processing.

Shown in Fig. 11 is a plot of ΔG^O versus σ_M. For charge densities in the region -20 to 0 $\mu C\,cm^{-2}$ the Gibbs energies of adsorption were calculated from the initial slopes of the surface pressure versus mole fraction of pyridine plots obtained at constant charge density as outlined in ref. 14. The Gibbs energies for $\sigma_M > 0$ were obtained by plotting the ϕ values versus $RTln(c)$ and subsequently shifting the curves corresponding to a given value of σ_M along the $RTln(c)$ axis to give the best overlap with the curve determined for σ_{max} ($+26\,\mu C\,cm^{-2}$). The Gibbs energy at σ_{max} was taken to be equal to the value of ΔG^O at E_{max} as shown in Fig. 8. The data presented in Fig. 11 show that the Gibbs energies of adsorption depend on σ_M in a pseudo parabolic way.

The consistency of our results can once again be checked by taking into consideration the following relationship obtained by cross differentiating the electrocapillary equation:

$$\left(\frac{\partial E}{\partial \Gamma}\right)_{\sigma_M} - \left(\frac{\partial \Delta G}{\partial \sigma_M}\right)_\Gamma \qquad (2)$$

According to the above expression, the first derivative of the Gibbs energy of adsorption with respect to the charge density (taken at constant Γ), should be equal to the slope of the electrode potential versus the surface excess plot (taken at constant σ_M). Figure 12 shows a plot of $\Delta_2^M \phi$ versus Γ taken at constant σ_M. $\Delta_2^M \phi$ is the potential drop across the inner layer region of the double layer which is given by the following equation:

$$\Delta_2^M \phi - E - E_{pzc} - \phi_2 \qquad (3)$$

where E_{pzc} is the potential of zero charge and ϕ_2 is the potential drop across the diffuse layer which is obtained from the classical Gouy-Chapman theory. At constant σ_M the derivative of $\Delta_2^M \phi$ with respect to Γ is equal to the derivative of E with respect to Γ. The plots presented in Fig. 12 are nonlinear. However, the limiting slopes of these curves taken at Γ → 0 progressively decrease with negative charge at the surface. The initial slopes of these curves are compared to the result of the numerical differentiation of the ΔG^o versus σ_M curve in Fig. 13. Although the scatter of the experimental points is large, satisfactory agreement between the two sets of data is observed indicating that no major errors were made in the data processing.

Summary and Conclusions

Data characterizing the adsorption of pyridine onto a Au(311) single crystal electrode surface have been presented. The data have been analyzed in terms of both

13

potential and charge. The important adsorption parameters are summarized in Table 1. The results show that pyridine adsorbs onto the Au(311) electrode surface in the vertical orientation over the entire potential (charge) region investigated. From the shift of the potential of zero charge one can conclude that the nitrogen end of the pyridine molecule is facing the metal surface. The fairly large values observed for the Gibbs energies of adsorption indicate that the pyridine molecules are weakly chemisorbed onto the Au(311) electrode surface. The consistency of our results has also been checked using expressions for the partial derivatives determined by cross differentiation of the electrocapillary equation. It can be concluded that our data are free from major errors which may have arisen as a result of data processing.

To conclude this paper we would like to stress briefly the similarities between pyridine adsorption at the Au(311) and Au(110) surfaces. The structure of the two surfaces consists of monatomic steps separated by two atom wide terraces. Using the TLK model, they can be denoted as (110) = 2(111) x (111) and (311) = 2(111) x (100) = 2(100) x (111). Consequently, the two planes can be considered as having the same type of steps but different terraces, or alternatively, different steps but the same terraces. The structural differences between the two planes are therefore small.

In an earlier contribution we reported on the adsorption of pyridine onto an Au(110) surface (4). The adsorption parameters obtained from that study are presented in Table 1 where they are compared to the data obtained here for the Au(311) plane.

Pyridine molecules assume only one - vertical orientation with the nitrogen end facing the metal on both the negatively and positively charged surfaces. The magnitude of all the adsorption parameters listed in Table 1 are comparable for the two planes. Clearly, pyridine adsorption onto the Au(311) and Au(110) surfaces is very similar and virtually unaffected by the small structural differences between these single crystal faces. Incidentally, similarities between pyridine adsorption at the (110) and (311) surfaces of silver have been observed recently in this laboratory (15). A more detailed discussion of the effect of surface crystallography on pyridine adsorption at gold electrodes will be presented in our next contribution in which results from adsorption studies on the (100), (110), (111), and the (311) planes of gold will be compared.

Acknowledgements

References

1. L. Stolberg, J. Richer, J. Lipkowski and D.E. Irish, J. Electroanal. Chem., 207 (1986) 213.

2. L. Stolberg, J. Lipkowski and D.E. Irish, J. Electroanal. Chem., 300 (1991)   .

3. L. Stolberg, J. Lipkowski and D.E. Irish, J. Electroanal. Chem., 238 (1987) 333.

4. L. Stolberg, J. Lipkowski and D.E. Irish, J. Electroanal. Chem., 296 (1990) 171.

5. L. Stolberg, S. Morin, J. Lipkowski and D.E. Irish, J. Electroanal. Chem. In Press.

6. J. Richer, L. Stolberg and J. Lipkowski, Langmuir, 2 (1986) 630.

7. J. Richer and J. Lipkowski, J. Electrochem. Soc., 133 (1986) 121.

8. A. Hamelin, J. Electroanal. Chem., 142 (1982) 299.

9. J. Lecoeur, J.P. Bellier and C. Koehler, Electrochim. Acta, 35 (1990) 1383.

10. R. Parsons, Proc. R. Soc. London Ser. A., 261 (1961) 79.

11. B.E. Conway, R.G. Barradas, P.G. Hamilton and J.M. Parry, J. Electroanal. Chem., 10 (1965) 485.

12. (a) D.M. Mohilner, H. Nakadomari and P. Mohilner, J. Phys. Chem., 81 (1977) 244; (b) J. Jastrzebska, M. Jurkiewicz-Herbich and S. Trasatti, J. Electroanal. Chem., 216 (1987) 21.

13. K.J. Vetter and J.W. Schultze, Ber. Bunsenges. Phys. Chem., 76 (1972) 920.

14. A. Iannelli, J. Richer and J. Lipkowski, Langmuir, 5 (1989) 466.

15.   A. Hamelin, S. Morin, J. Richer and J. Lipkowski, J. Electroanal. Chem., <u>285</u> (1990) 249.

Figures

Fig. 1.   Cyclic voltammograms recorded for (a) 0.1 M $KClO_4$ and (b) 0.1 M $KClO_4$ + 3 x 10^{-4} M pyridine. Sweep rate = 20 mV s^{-1}.

Fig. 2.   Differential capacity curves recorded for Au(311) in the presence of the supporting electrolyte (0.1 M $KClO_4$) as well as the various pyridine concentrations indicated. Sweep rate = 5 mV s^{-1} and the ac modulation frequency is 25 Hz.

Fig. 3.   Charge density-potential curves which have been obtained for the following pyridine concentrations: (●) 2 x 10^{-3} M; (O) 10^{-3} M; (✳) 3 x 10^{-4} M; (□) 10^{-4} M; (x) 7 x 10^{-5} M; (▲) 3 x 10^{-5} M; (△) 2 x 10^{-5} M; (⊙) 10^{-5} M; (▣) 5 x 10^{-6} M; (·) 0.

Fig. 4.   Film pressure versus electrode potential curves for the following pyridine concentrations: (1) 2 x 10^{-3} M; (2) 10^{-3} M; (3) 3 x 10^{-4} M; (4) 10^{-4} M; (5) 7 x 10^{-5} M; (6) 3 x 10^{-5} M; (7) 2 x 10^{-5} M; (8) 10^{-5} M; (9) 5 x 10^{-6} M.

Fig. 5.   Surface pressure versus absolute charge density curves obtained for the following pyridine concentrations: (O) 2 x 10^{-3} M; (●) 10^{-3} M; (△) 3 x 10^{-4} M; (▲) 10^{-4} M; (□) 7 x 10^{-5} M; (■) 3 x 10^{-5} M; (▽) 2 x 10^{-5} M; (▼) 10^{-5} M; (◇) 5 x 10^{-6} M.

Fig. 6.   (a) Surface concentration-potential curves obtained for the following pyridine concentrations: (1) 2 x 10^{-3} M; (2) 10^{-3} M; (3) 3 x 10^{-4} M;

18

(4) 10^{-4} M; (5) 7×10^{-5} M; (6) 3×10^{-5} M; (7) 2×10^{-5} M; (8) 10^{-5} M and

(b) the corresponding adsorption isotherms which have been obtained at

the following electrode potentials: (1) -0.55 V; (2) -0.50 V; (3) -0.45 V;

(4) -0.40 V; (5) -0.35 V; (6) -0.30 V; (7) -0.25 V; (8) -0.20 V; (9) -0.15 V;

(10) -0.10 V; (11) -0.05 V.

Fig. 7.   (a) Surface concentration-charge density curves for the following pyridine

concentrations: (1) 10^{-3} M; (2) 3×10^{-4} M; (3) 10^{-4} M; (4) 7×10^{-5} M; (5)

3×10^{-5} M; (6) 2×10^{-5} M; (7) 10^{-5} M and (b) the corresponding

adsorption isotherms which have been obtained for the various charge

densities in $\mu C\ cm^{-2}$ indicated.

Fig. 8.   Plot of ΔG^{o} versus E as determined from the Henry's Law isotherm.

Fig. 9.   Plots of σ_M versus Γ obtained at the following electrode potentials:

(●) -0.55 V; (O) -0.45 V; (■) -0.35 V; (□) -0.25 V; (▲) -0.20 V; (△) -0.15 V;

(♦) -0.10 V; (◊) -0.05 V.

Fig. 10.   Dependence of the electrosorption valencies on the electrode potential. (□)

determined from the slope of the σ_M versus Γ plots and (O) by numerical

differentiation of the ΔG^{o} versus E curve corresponding to Henry's Law.

Fig. 11.   Plot of ΔG^{o} versus σ_M as determined from the Henry's law isotherm.

Fig. 12.   Plots of $\Delta_2^{M}\phi$ versus Γ for the following charge densities indicated: (O) -20

$\mu C\ cm^{-2}$; (●) -16 $\mu C\ cm^{-2}$; (□) -12 $\mu C\ cm^{-2}$; (■) -8 $\mu C\ cm^{-2}$;

19

(Δ) -4 μC cm^{-2}; (▲) 0; (▽) +4 μC cm^{-2}; (▼) +8 μC cm^{-2}; (◊) +12 μC cm^{-2}.

Fig. 13.   Comparison of the dependence of $(\partial\Delta_2^M\phi/\partial\Gamma)_\sigma$ on the charge density determined from the initial slopes of the plots presented in Fig. 12. (O) and by numerical differentiation of the ΔG^O versus σ_M curve presented in Fig. 11. (■).

Table 1. Adsorption parameters for pyridine adsorbed onto the (311) and (110) faces of gold.

Parameters	Au(311)	Au(110)
E_{max} / V	+0.39	+0.23
E_{pzc} / V	+0.020	-0.015
$(E_{max} - E_{pzc})$ / V	+0.37	+0.25
σ_{max} / $\mu C\ cm^{-2}$	+28	+24
E_N / V	-0.73	-0.65
$10^{10}\Gamma_{max}$ / mol cm^{-2}	6.6	6.1
ΔG^{o}_{max} / kJ mol^{-1}	-44	-42

Fig. 1

Fig. 2

0.1 M KClO₄

2x10⁻³ M Pyridine

10⁻³ M Pyridine

10⁻⁴ M Pyridine

C / μF cm⁻²

E / V
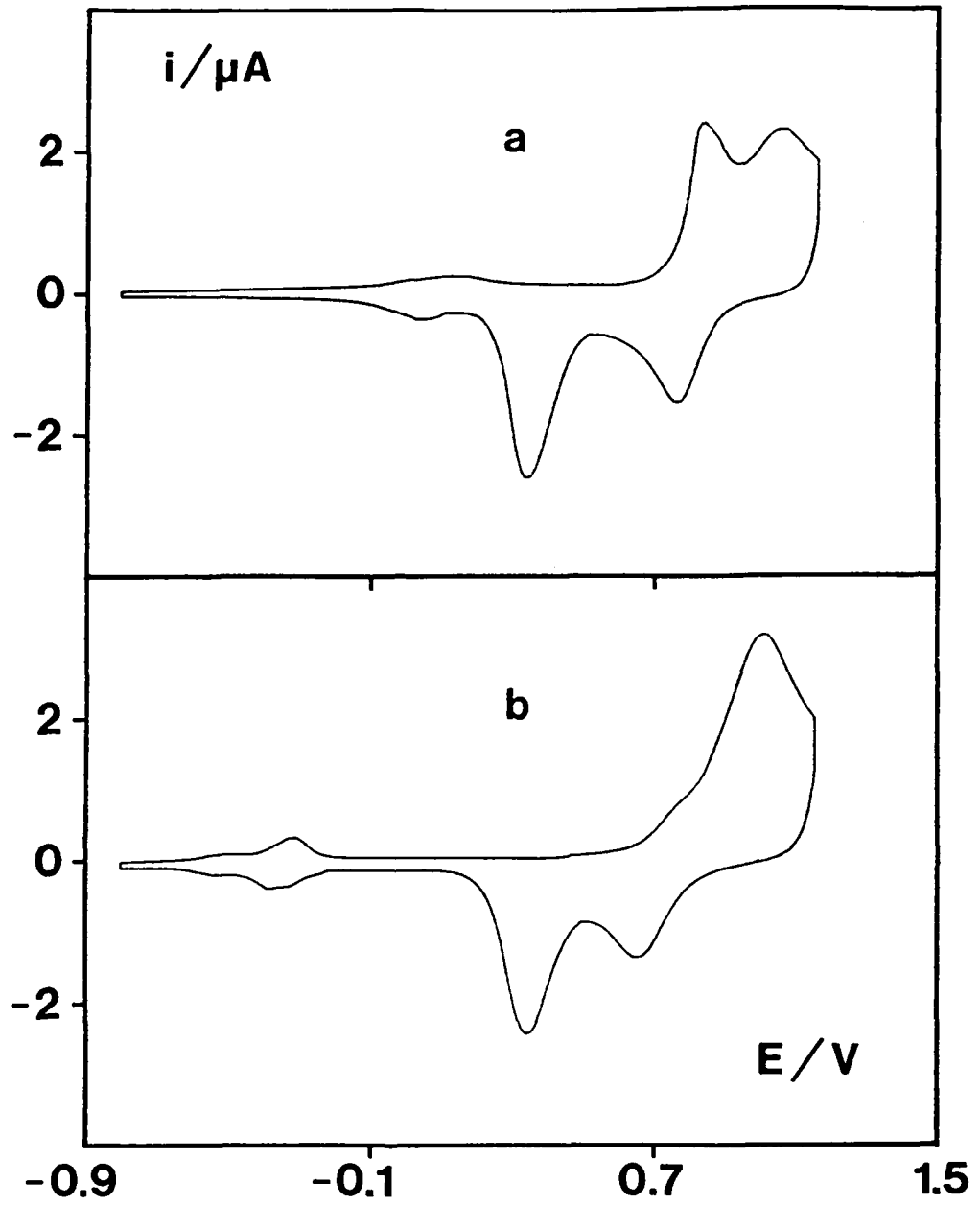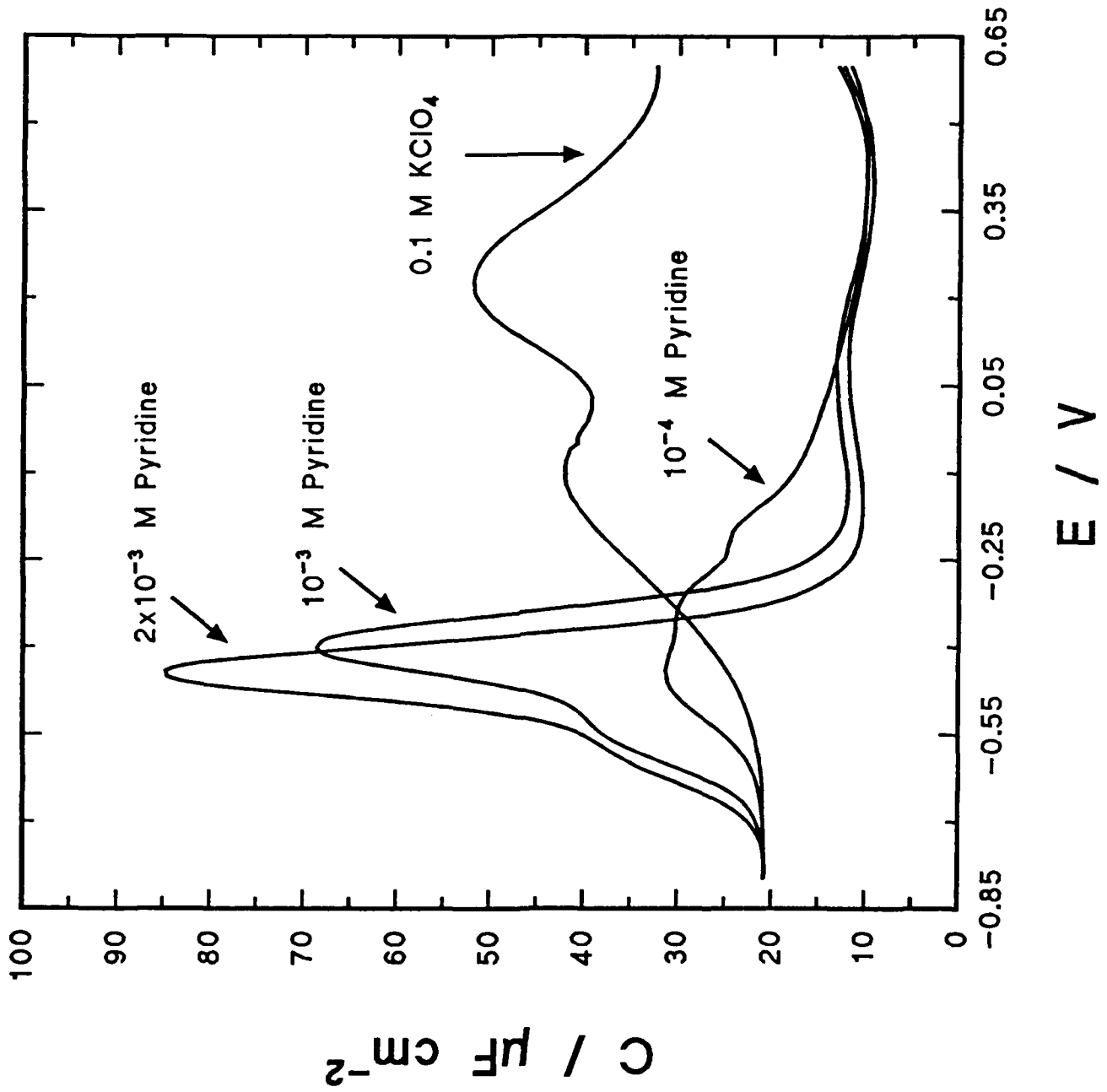
Fig. 3

Fig. 4.

Fig. 5

Fig. 6a

Fig. 65

Fig. 7a

Fig. 7b.
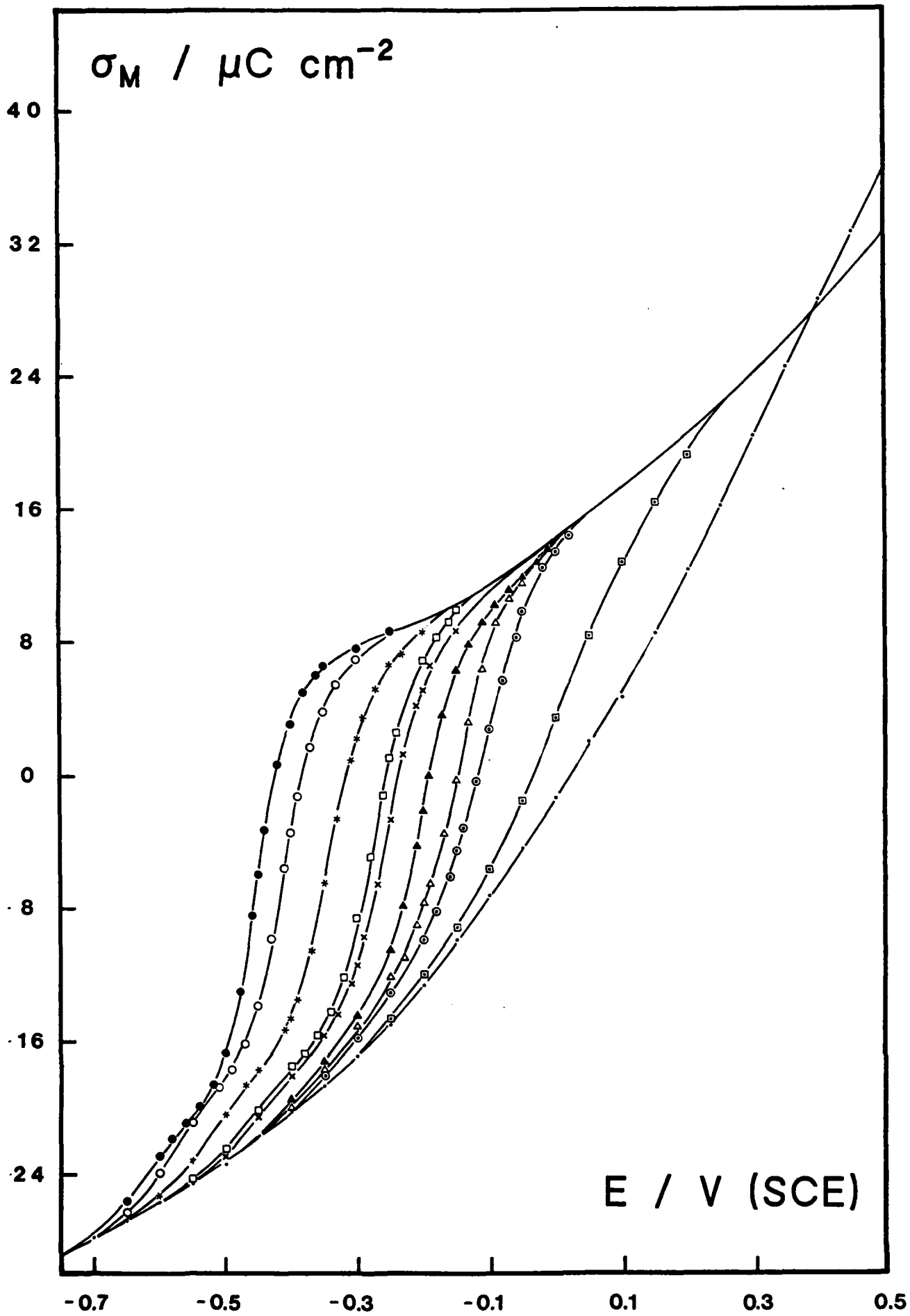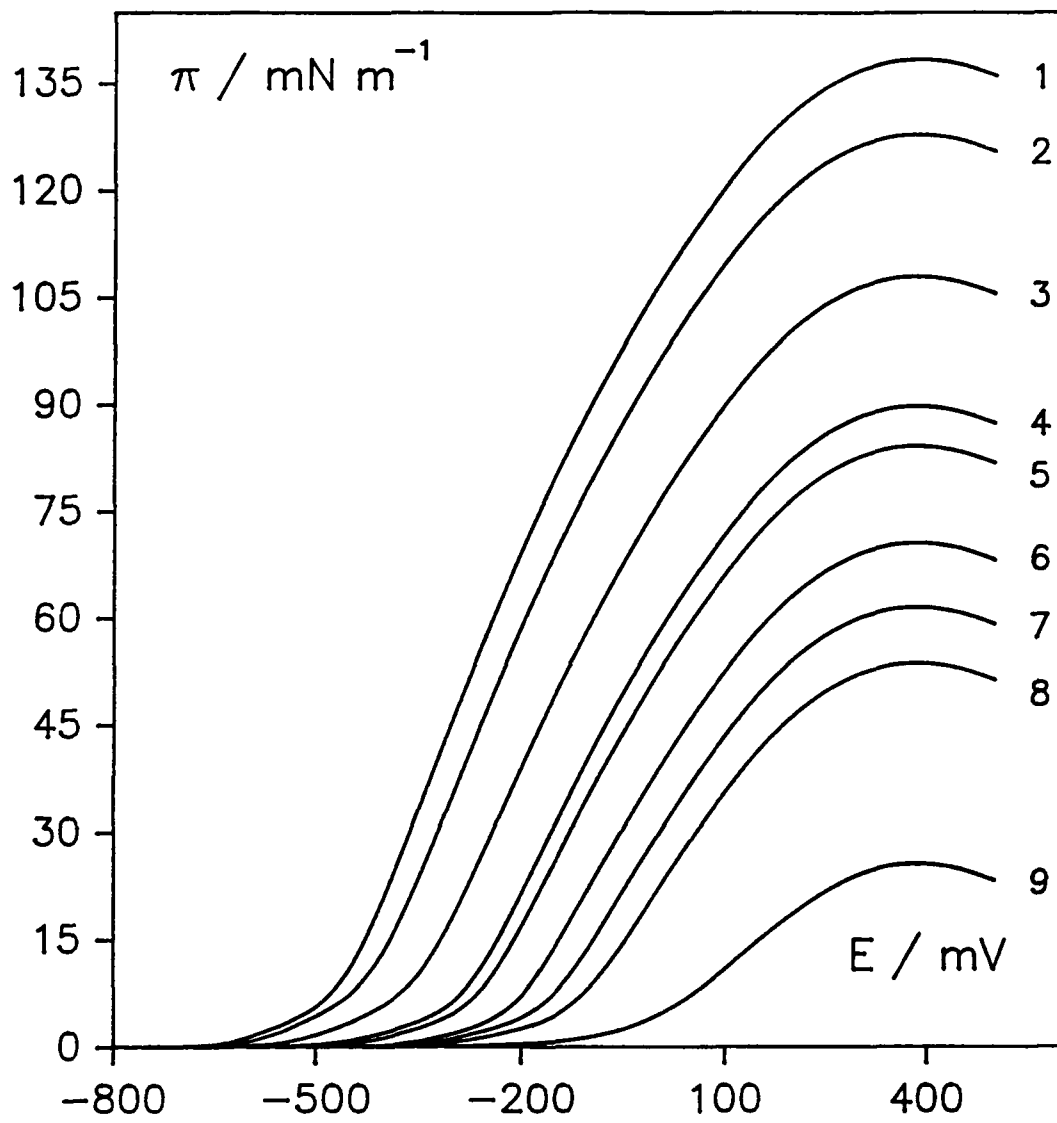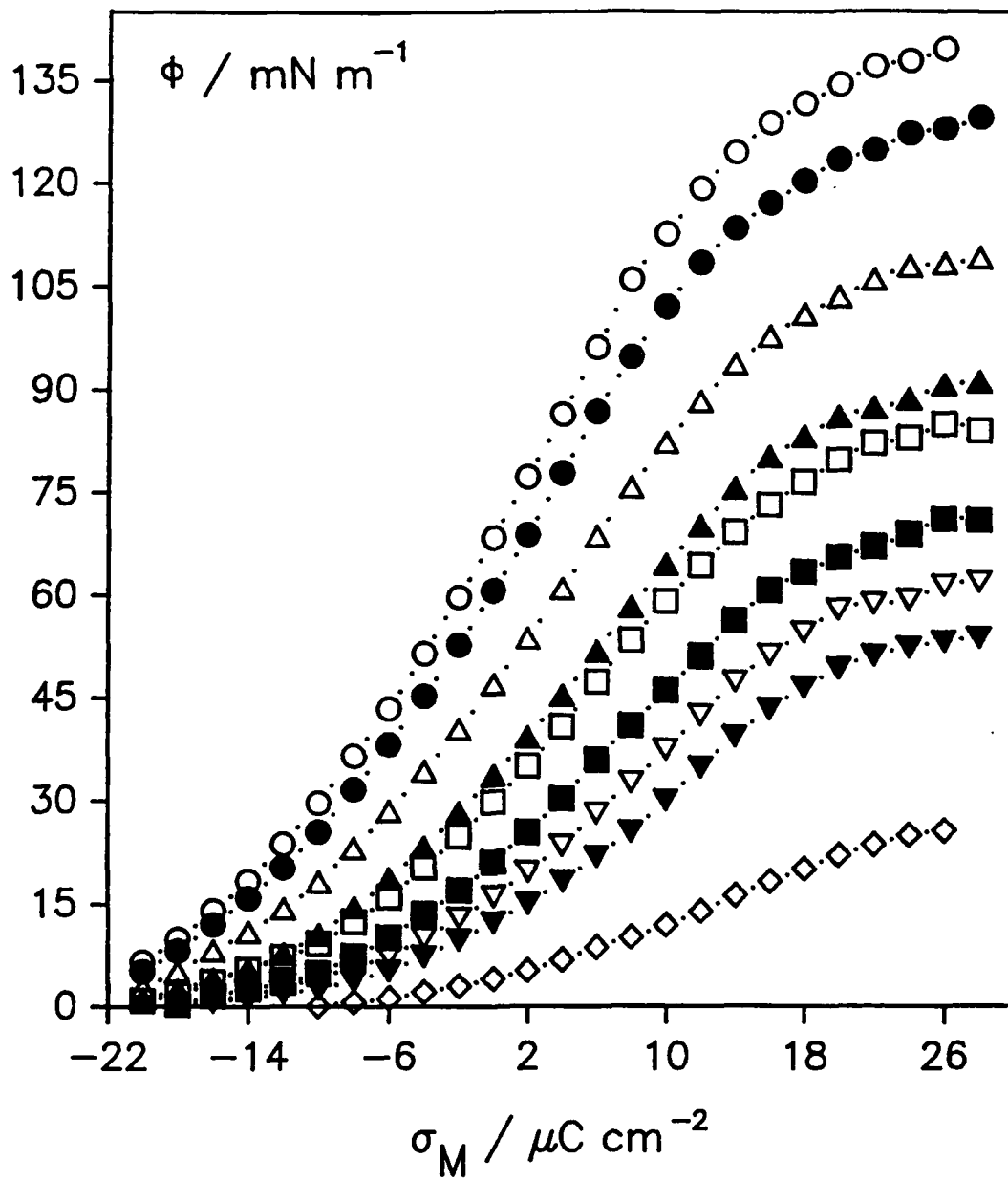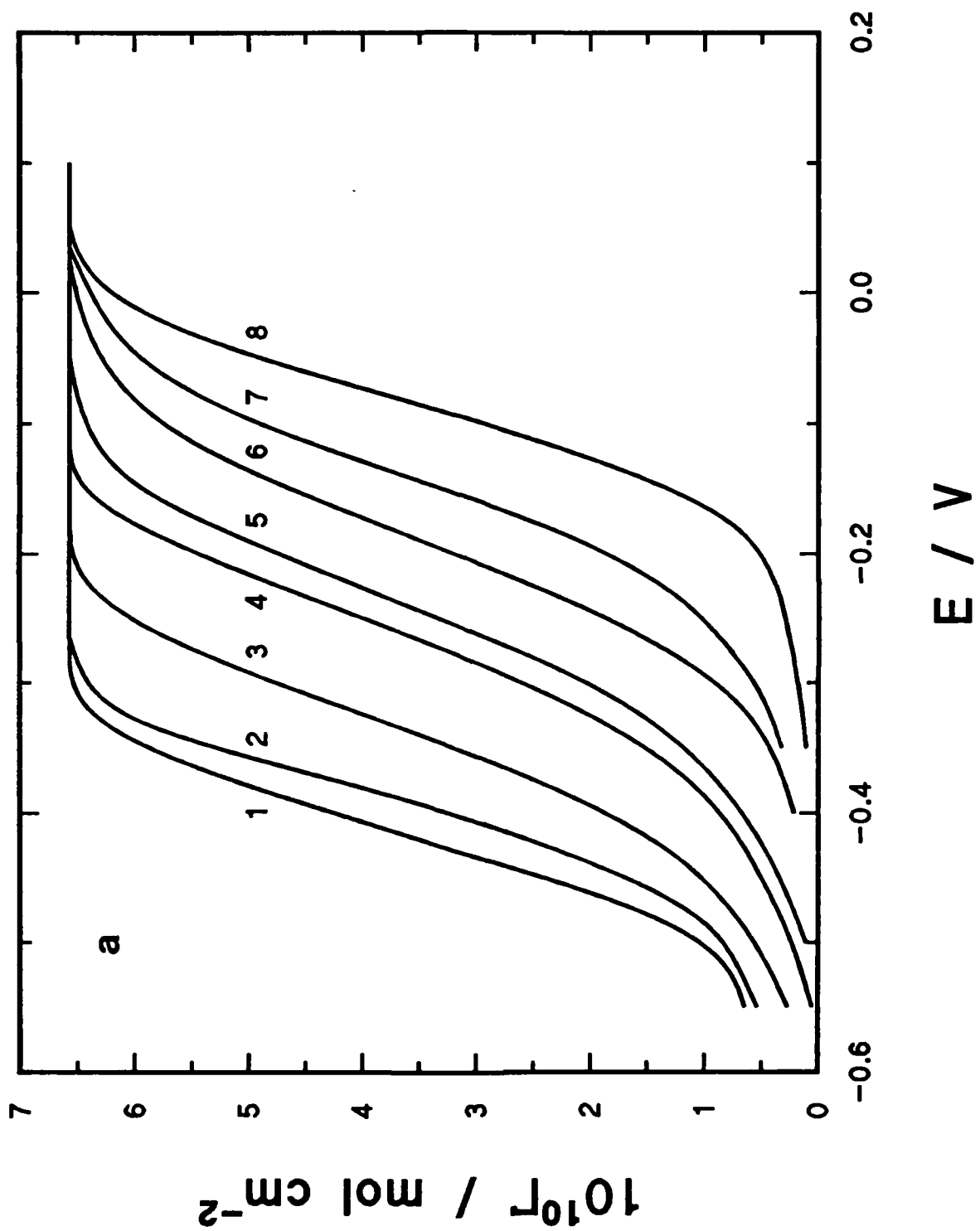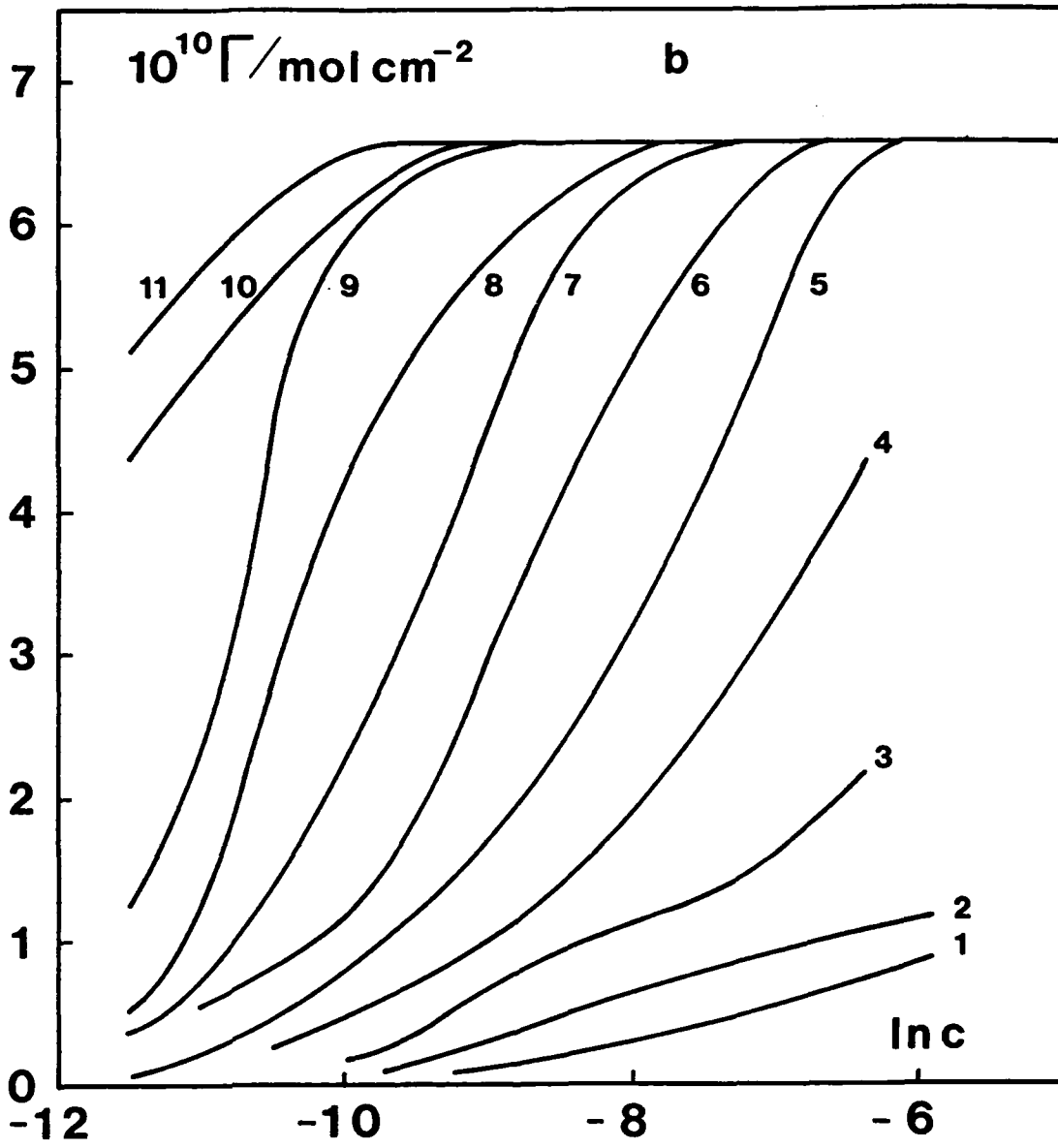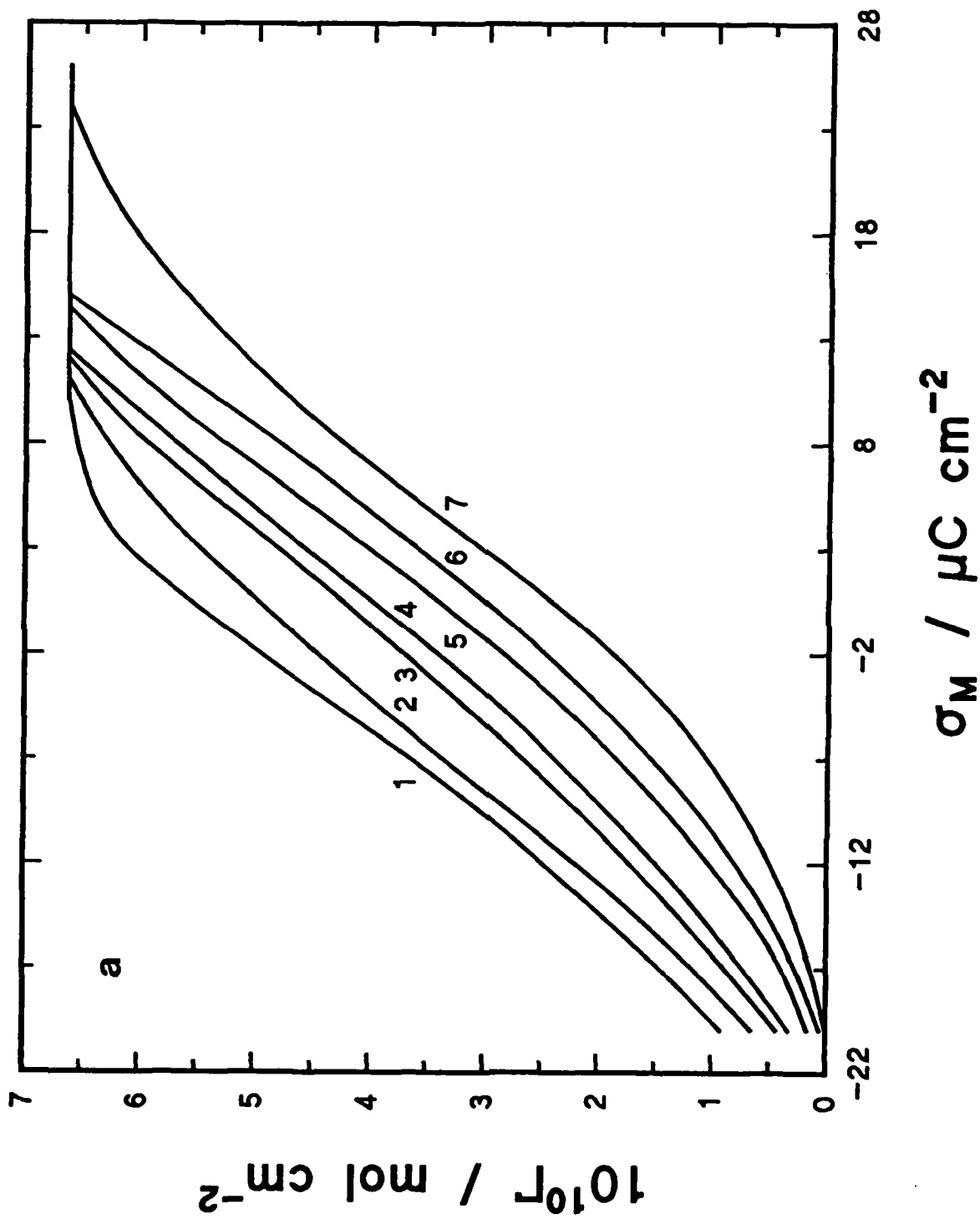
Fig. 8

Fig. 9

Fig. 10

Fig. 11

σ_M / μC cm^{-2}

$-\Delta G^\circ$ / kJ mol^{-1}
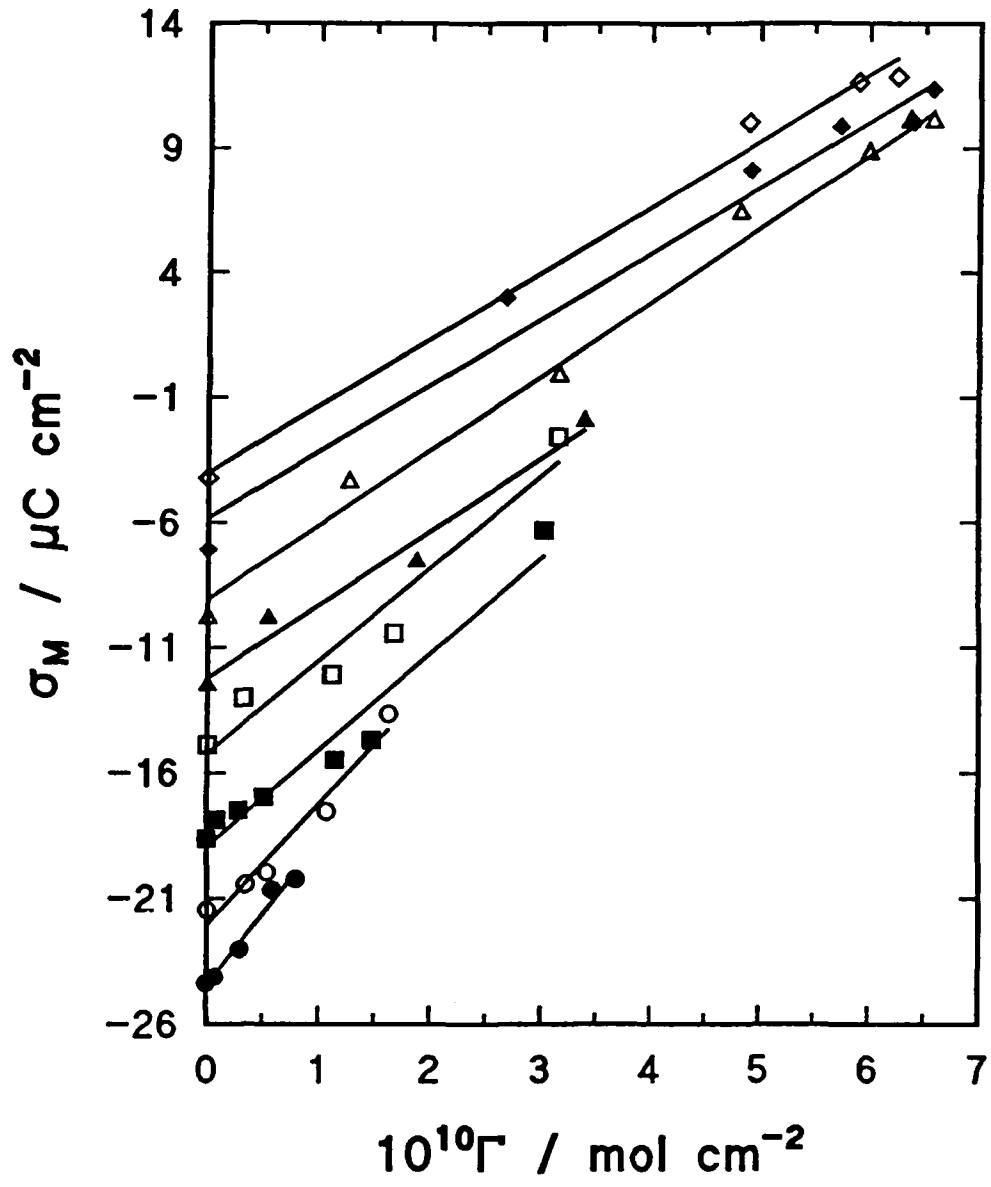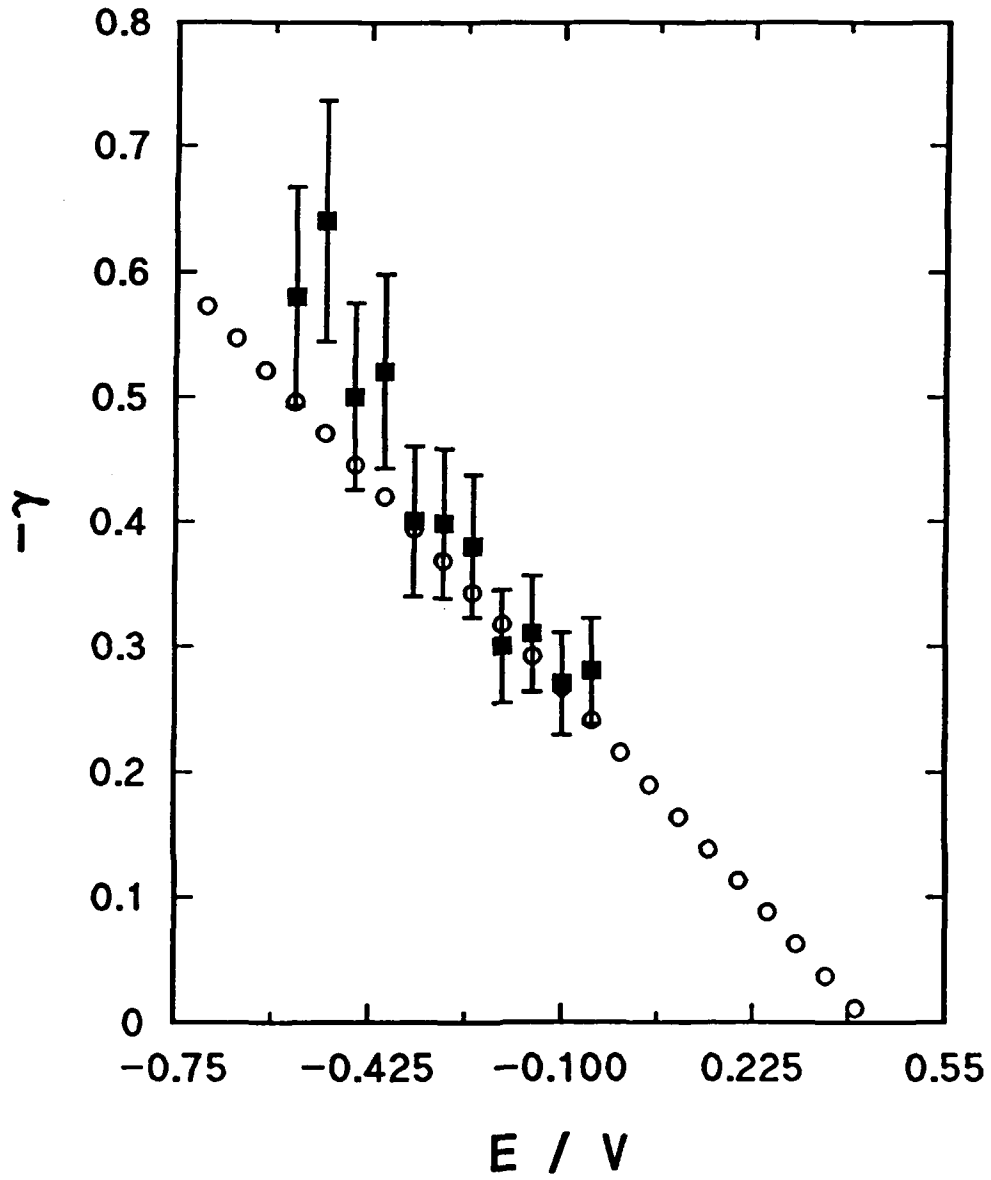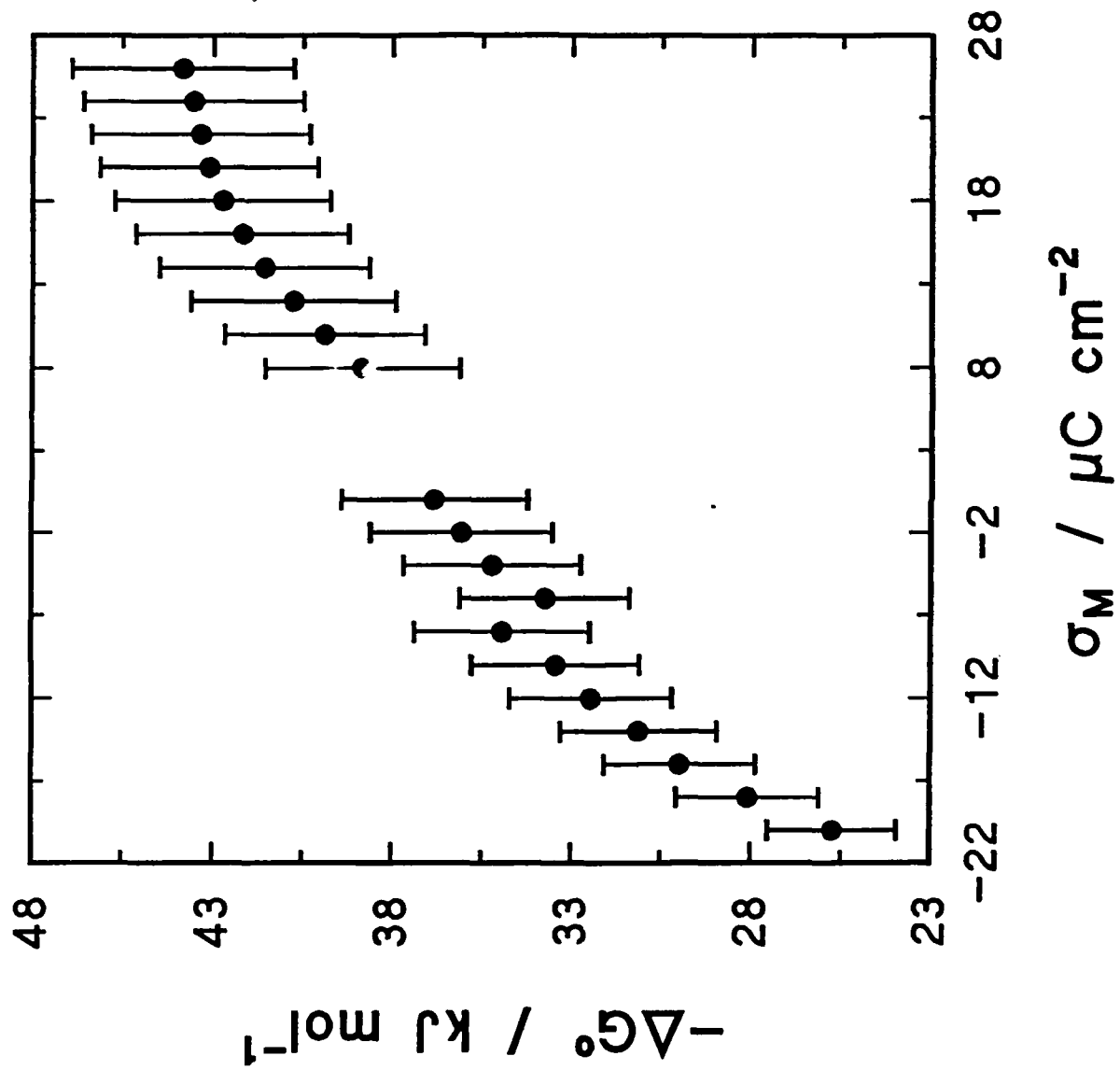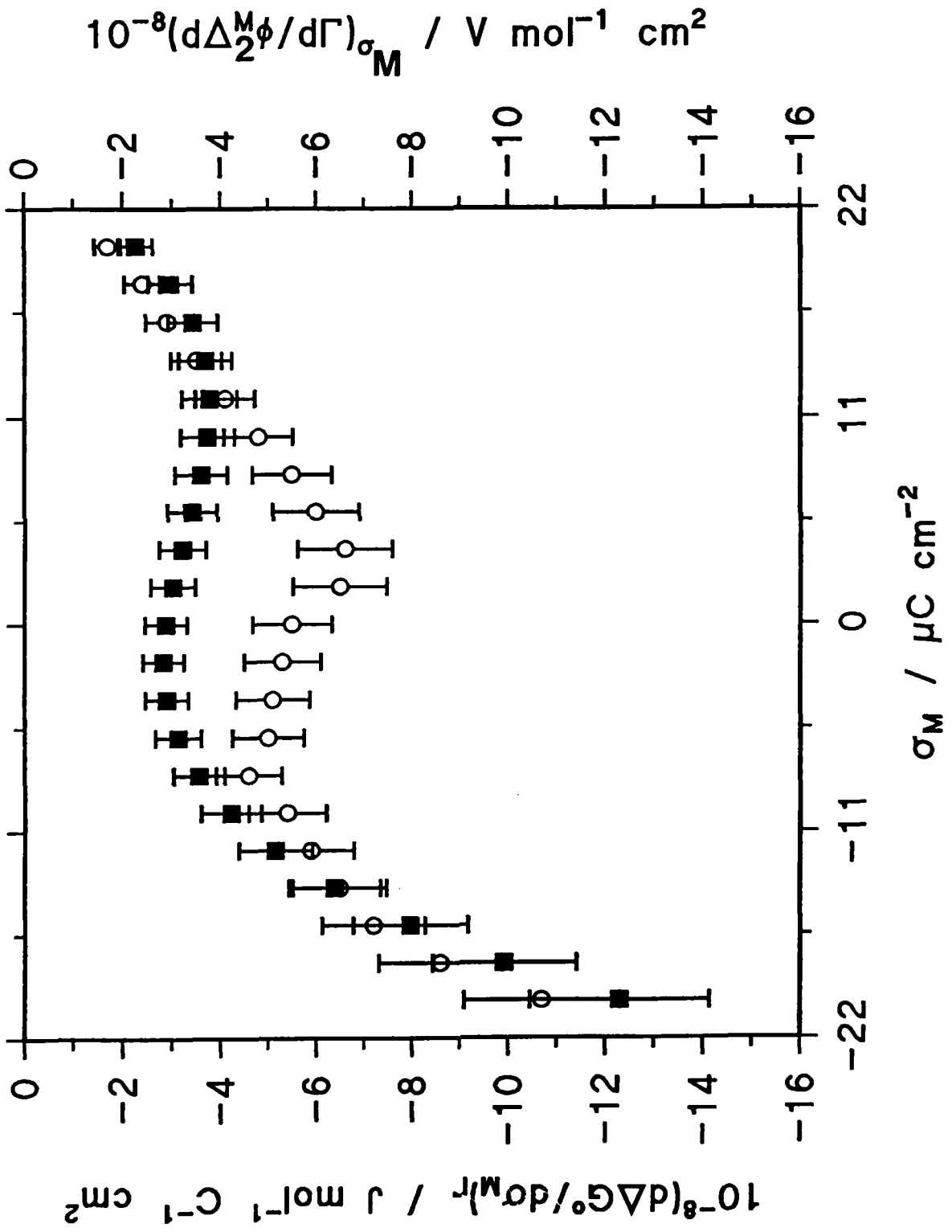
Fig. 12

Fig. 12.
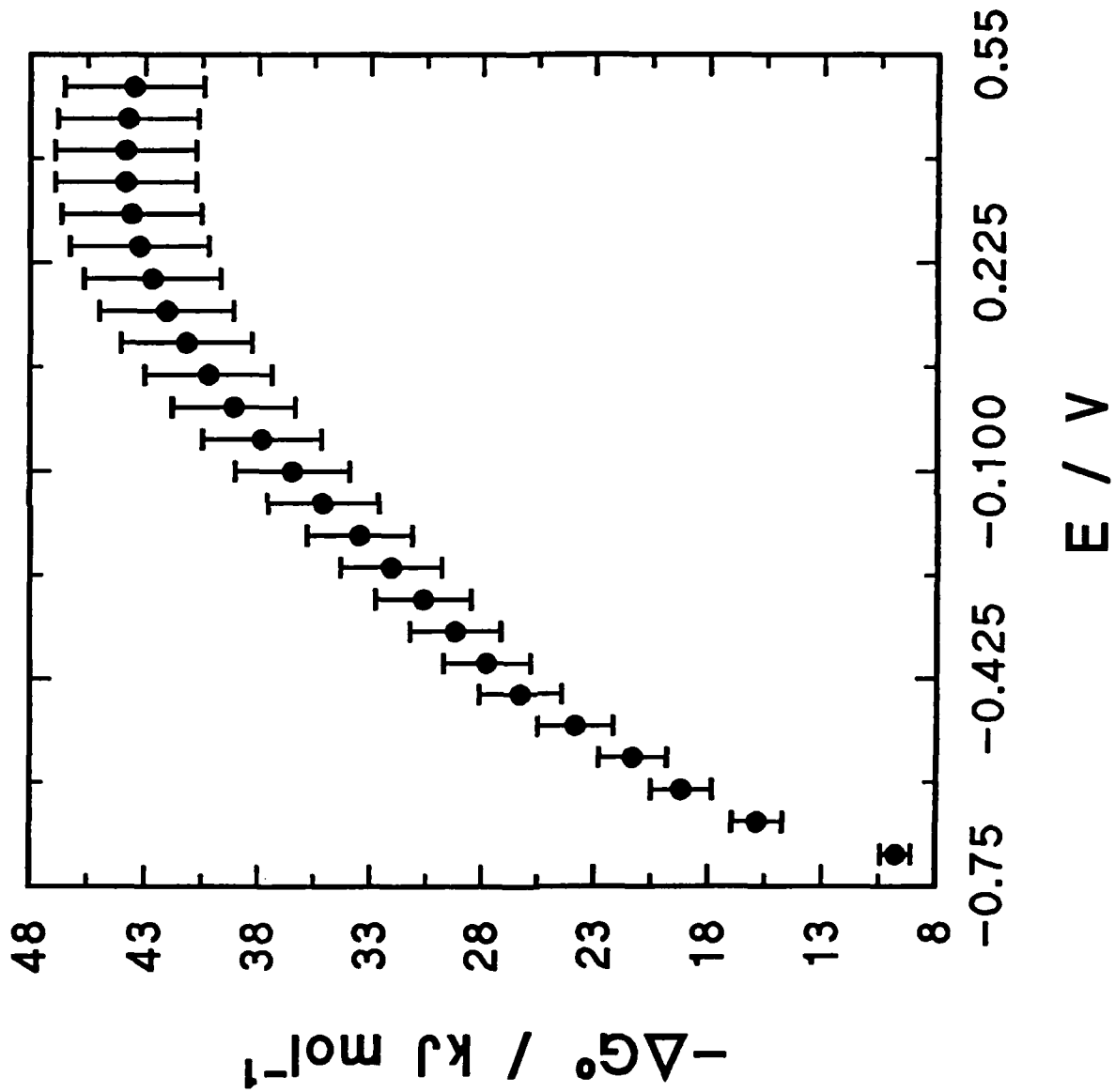
TECHNICAL REPORT DISTRIBUTION LIST - GENERAL

Office of Naval Research   (2)
Chemistry Division, Code 1113
800 North Quincy Street
Arlington, Virginia 22217-5000

Dr. Robert Green, Director (1)
Chemistry Division, Code 385
Naval Weapons Center
China Lake, CA 93555-6001

Commanding Officer   (1)
Naval Weapons Support Center
Dr. Bernard E. Douda
Crane, Indiana 47522-5050

Chief of Naval Research   (1)
Special Assistant for Marine
    Corps Matters
Code 00MC
800 North Quincy Street
Arlington, VA 22217-5000

Dr. Richard W. Drisko   (1)
Naval Civil Engineering
 Laboratory
Code L52
Port Hueneme, CA 93043

Dr. Bernadette Eichinger   (1)
Naval Ship Systems Engineering
    Station
Code 053
Philadelphia Naval Base
Philadelphia, PA 19112

David Taylor Research Center (1)
Dr. Eugene C. Fischer
Annapolis, MD 21402-5067

Dr. Sachio Yamamoto   (1)
Naval Ocean Systems Center
Code 52
San Diego, CA 92152-5000

Dr. James S. Murday   (1)
Chemistry Division, Code 6100
Naval Research Laboratory
Washington, D.C. 20375-5000

Dr. Harold H. Singerman   (1)
David Taylor Research Center
Code 283
Annapolis, MD 21402-5067

Defence Technical Information (2)
    Center
Building 5
Cameron Station
Alexandria, VA
U.S.A.   22314